Macromolecules
ARTICLE

Macromolecules **2010**, *43*, 3081–3089 **3081**
DOI: 10.1021/ma902689c

Coil−Stretch Transition of DNA Molecules in Slitlike Confinement

Jing Tang, Daniel W. Trahan, and Patrick S. Doyle*

Department of Chemical Engineering, Massachusetts Institute of Technology, Cambridge, Massachusetts 02139

Received December 4, 2009; Revised Manuscript Received January 26, 2010

ABSTRACT: We experimentally investigate the influence of slitlike confinement on the coil−stretch transition of single DNA molecules in a homogeneous planar elongational electric field. We observe a more gradual coil−stretch transition characterized by two distinct critical strain rates for DNA in confinement, different from the unconfined case where a single critical strain rate exists. We postulate that the change in the coil−stretch transition is due to a modified spring law in confinement. We develop a dumbbell model to extract an effective spring law by following the relaxation of an initially stretched DNA. We then use this spring law and kinetic theory modeling to predict the extension and fluctuations of DNA in planar elongational fields. The model predicts that a two-stage coil−stretch transition emerges in confinement, in accord with experimental observations.

1. Introduction

Advances in nanofabrication technologies have inspired interest in nanodevices that promise to provide fast and accurate methods for the analysis of genomic length DNA. Many such applications, including DNA separation[1,2] and single molecule mapping,[3,4] rely on the ability to stretch individual DNA molecules from their initial coiled configurations into extended states. Understanding how polymer deforms under confinement is therefore of considerable importance for device design and optimization. Meanwhile, such knowledge can also aid to the development of fundamental polymer physics. The unique advantage of using nanoconfinement to stretch DNA lies in its capability to alter the shape and dynamics of polymers through both steric interactions and modulation of intramolecular hydrodynamic interactions (HI).[5−8] Recent studies have used tubelike confinement (representing channels with height ≈ width) to substantially change the equilibrium DNA conformation from a coil to a highly extended state.[4,9−13] Alternatively, slitlike confinement (representing channels with height ≪ width) has been employed to facilitate stretching DNA far from equilibrium in elongational fields.[14] In this case the polymer deformation results from the competition between the stretching force imposed by the field gradients and the DNA elastic spring force that resists stretching.[15] In contrast to the equilibrium behavior of confined polymer that has gained much attention to date (see ref 16 for a review), the influence of confinement on this nonequilibrium process has only recently begun to be examined. Initial studies in this field[14,17] have demonstrated a unique feature of DNA stretching in slitlike nanochannels: the steric interactions between DNA and the confining walls become weaker and eventually vanish as the molecule extends, suggesting that the stretching process may be conformation-dependent.

Several experimental studies have investigated the stretching of unconfined DNA in extensional hydrodynamic flows[18−22] and electric fields.[23,24] A sudden increase in the steady-state extension of DNA was observed near a critical velocity (electric field) gradient or strain rate of $\dot{\varepsilon}_c$. The values of $\dot{\varepsilon}_c$ determined in these experiments agree well with the theoretical prediction of $\dot{\varepsilon}_c \approx 0.5/\tau$, where τ is the longest relaxation time of the polymer.[25] The abrupt coil−stretch transition is closely related to the shape of the spring force law.[18] For DNA in bulk, the force law is characterized by a linear force regime from equilibrium to ∼30% relative extension and a highly nonlinear response at large extensions (see Figure 1B). For $\dot{\varepsilon} < \dot{\varepsilon}_c$, the stretching force exerted on the polymer is lower than the spring force, and thus the conformation is weakly perturbed. As soon as the strain rate is increased above $\dot{\varepsilon}_c$, the stretching force exceeds the linear portion of the spring force, and the polymer stretches into a significantly extended state until its nonlinear elasticity limits any further extension. During this conformational transition, polymer molecules also exhibit slowed-down transient dynamics toward steady-state and an increased magnitude of extension fluctuations,[22,26,27] similar to the critical phenomena observed in a thermodynamic phase transition. The essential physical reason for these unique behaviors is the existence of large number of configurations corresponding to vastly different extensions that are accessible close to the critical strain rate, at which the stretching force balances the entire linear region of the elastic spring force.[22] In potential flows, this configuration space can also be interpreted in terms of a conformational energy landscape[15] that becomes relatively flat near the coil−stretch transition. The aforementioned characteristics of the coil−stretch transition, i.e., the drastic deformation, the dynamic slowdown, and the significant conformation fluctuations, are enhanced by the extension-dependent hydrodynamic drag coefficient, a result of the dominant intramolecular HI for DNA in bulk.[15,20−22,27] The drag coefficient of the polymer directly impacts on the stretching force imposed by the field gradients. An extremely large increase in the drag coefficient as the polymer fully extends from the coiled state can lead to conformational hysteresis at the coil−stretch transition.[15,20]

Slitlike nanochannels offer a very powerful method to change the course of DNA deformation by impacting both the applied stretching force and the DNA spring force. The stretching force is affected through modulation of intromolecular HI: nanoslits with height smaller than the equilibrium size of DNA are capable of screening long-range HI, leading to an increased drag coefficient of DNA and thus stronger stretching force.[28,29] Meanwhile, the increase in drag coefficient is more dramatic for coiled DNA

*Corresponding author. E-mail: pdoyle@mit.edu.

Published on Web 02/23/2010

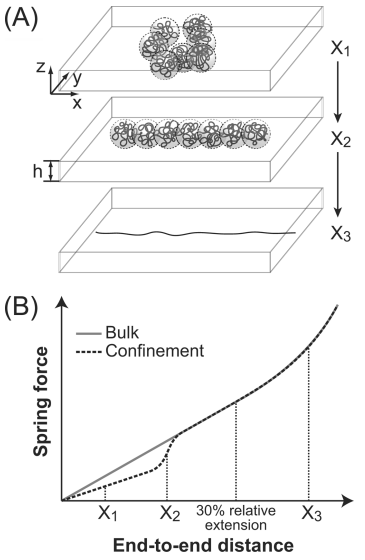

Figure 1. (A) Schematic of the DNA stretching process in slitlike nanochannels. (B) Schematic comparison of the effective spring force law for DNA in confinement and in bulk. The bulk spring force varies linearly with the end-to-end distance below ~30% relative extension. In confinement, DNA molecules near equilibrium are sterically confined, and the corresponding spring force is reduced. Highly extended DNA is no longer confined, and the spring force restores back to the bulk force law.

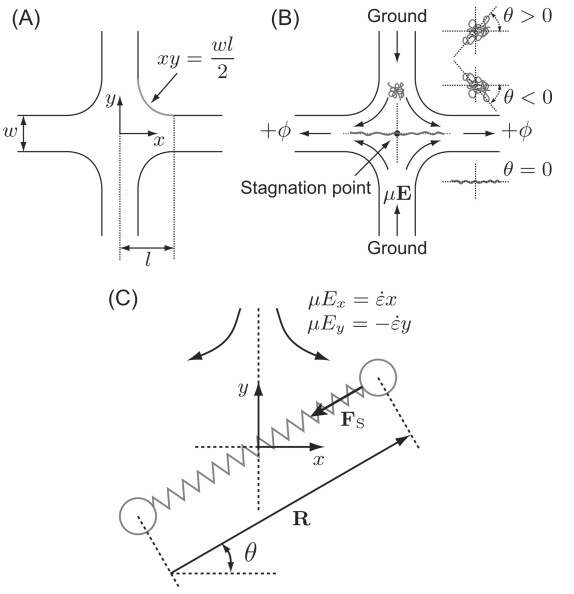

Figure 2. (A) Diagram of the cross-slot stretching device geometry. The geometrical parameters of the channels used in this study are summarized in Table 1. (B) Schematic of the motion and stretching of DNA molecules in the device. Independent applied voltages to the left and right arms of the channel allow adjustment of the location of the stagnation point and trapping of the DNA molecules. Also shown is the geometrical setup for the measurement of the angle of the principal axis of the radius of gyration (θ). (C) Setup of the Brownian dumbbell model in a planar homogeneous extensional electric field. The center of mass of the dumbbell is fixed at the stagnation point.

than that for highly extended molecule, hence the overall extension dependence of the drag coefficient is significantly reduced. Modification of the DNA spring force relies on the steric interactions between DNA and the confining walls, which, however, are only important for DNA molecules at moderate extensions.[17] A highly extended DNA is not sterically confined in the nanochannels, and the corresponding spring force stays unaffected (i.e., identical to the bulk spring force; see Figure 1). As the extension decreases, the lateral dimension of the DNA (z-dimension in Figure 1A) grows until it becomes equivalent to the channel height h. After this point, the conformation of the DNA is constrained by the steric confinement and the spring force is reduced. In nanochannels much taller than the persistence length of the DNA, this transition occurs within the bulk linear force regime (i.e., below 30% fractional extension),[14] and the spring force for confined DNA near equilibrium is still linear with extension but the spring constant is smaller.[7,30] As a result, the spring force law of DNA in slitlike confinement contains two linear regimes: a confined linear force regime close to equilibrium and a truncated bulk linear force regime at larger extensions (see Figure 1B), which are connected by a transition region where the spring force gradually restores to the bulk force law as the DNA stretches. The relative widths of these regions depend upon the channel height h.[14,17] The compound effect of the more uniform drag coefficient and the newly introduced conformation dependence in the spring force of DNA under confinement results in a very different stretching process. In the confined linear spring force regime, DNA molecules can be more easily deformed due to the increased drag coefficient and softened spring, pointing to the fact that confinement may allow a much earlier coil−stretch transition. As the DNA extends into the transition region, the spring stiffens and acts to limit the amount of extension. Once the DNA becomes nonsterically confined, stretching progresses as if the DNA were in bulk but with an increased drag coefficient. We have previously shown experimental evidence of this "bulklike" deformation at large extensions and found that despite the fact that the spring force in this region does not differ from the bulk force law, the increased drag coefficient reduces the strain rate required to stretch DNA to a certain extension.[14] The purpose of this study is to investigate the coil−stretch transition that takes place at moderate extensions where the DNA spring force is affected by the steric confinement. The existence of two linear spring force regimes with distinct spring constants foreshadows that confinement will both quantitatively and qualitatively modify coil−stretch transition.

2. Experiments

2.1. Device Geometry. We electrophoretically stretched single DNA molecules in homogeneous extensional electric fields under varying degrees of confinement. In a planar homogeneous extensional electric field, the electrophoretic velocity of a point charge varies linearly with position:

$$v_x = \mu E_x = \dot{\varepsilon} x \tag{1}$$

$$v_y = \mu E_y = -\dot{\varepsilon} y \tag{2}$$

where v_x and v_y are the velocities in the x and y directions, respectively, E_x and E_y are the electric fields in the x and y directions, respectively, μ is the electrophoretic mobility, and the strain rate $\dot{\varepsilon}$ is a constant. This type of field kinematics was achieved by applying symmetric potentials to a cross-slot channel with the incorporation of hyperbolically curved sidewalls (see Figure 2A,B). Since the shape of the sidewalls matches exactly the streamlines in a planar homogeneous extensional field, there are no inhomogeneities to disrupt the linear electric field profile over the entire intersection region.[31] For the same planar geometry ($x-y$ plane), the field lines do not depend on channel height so long as the height is uniform within a device. The channel has been recently used to study stretching of confined DNA at large extensions.[14] A unique feature of the device is that it allows for extremely long residence time (t_{res}) of DNA in the extensional electric field so that any molecular individualism effects[18,19] can be overcome, and the steady-state behaviors of DNA can be observed. The long residence time was

achieved by applying independently controlled potentials to the side reservoirs and thus enabling sensitive adjustment of the stagnation point position via perturbations to the field (see Figure 2B). With this capability of stagnation point control, any DNA molecules of interest can be trapped at the stagnation point for very high accumulated strains ($\varepsilon = \dot{\varepsilon} t_{res}$).

2.2. Channel and DNA Preparation. Cross-slot channels with three different heights were used in this study. 2 μm tall microchannels were constructed in polydimethylsiloxane (PDMS, Sylgard 184, Dow Corning) using soft lithography on a silicon master (SU8-2 photoresist). The PDMS channels were soaked in 0.5 × Tris-Boric acid-EDTA (TBE, Omnipure) buffer at 40 °C overnight to eliminate permeation driven flow through the PDMS,[32] rinsed and dried briefly, and sealed to a glass coverslide. Glass nanochannels with two different heights (h = 300 and 150 nm) were created by a photoresist protected etch in buffered oxide etchant and thermally bonded to a glass cover slide as described previously.[33] The glass nanochannels were filled with filtered deionized water and rinsed via application of potentials at the fluid reservoirs before use. All channels were flushed with the experimental buffer prior to exposure to DNA molecules. The experimental buffer was 0.5 × TBE solution with 0.1% 10 kDa polyvinylpyrrolidone (PVP, Polysciences) and an oxygen scavenger system consisting of 4 vol % β-mercaptoethanol (BME, Cabiochem), 12.5 mg/mL glucose (Mallinckrodt), 0.16 mg/mL glucose oxidase (Sigma), and 9.6 μg/mL catalase (Sigma). Channels were flushed with new buffer every 2 h during experiments to ensure a constant ionic strength environment.[34] T4 DNA molecules (165.6 kbp, Nippon gene) and λ-DNA molecules (48.502 kbp, New England Biolabs) were stained (at a DNA concentration of 0.69 μg/mL) with YOYO-1 (Invitrogen) dye at a base pair to dye ratio of 4:1 and allowed to sit at least overnight. DNA samples were diluted 2−10-fold immediately before experiments to reach an optimal concentration for observation.

2.3. DNA Stretching Experiments. Prior to each stretching experiment, the electric field kinematics in every channel were experimentally verified, and the strain rate was calibrated against applied voltage by tracking the center of mass of electrophoresing λ-DNA as described previously[14] (see Supporting Information for details). T4 DNA was used for the stretching experiments. A typical molecule was electrophoretically driven into the channel intersection, trapped at the stagnation point, and observed for 9 min or at least 20 units of strain at desired strain rate. The time constraint is to limit photobleaching of and photoinduced damage to the stained DNA molecules. We used an inverted Zeiss Axiovert 200 microscope with a 63× 1.4 NA oil-immersed objective to observe single DNA molecules. Images were captured using a Hamamatsu EB-CCD camera (model 7190-21) and NIH image software. The maximum extension of the DNA was measured from a simple threshold, and the angle of the principal axis of the DNA radius of gyration tensor with respect to the axis of elongation was extracted following procedures described in ref 30. For each strain rate studied, images of 25−35 DNA molecules were taken. Steady-state DNA configurations were sampled from each individual traces at time intervals equal to the higher extension relaxation time τ_I (see section 3.2 for definition) after the molecule has experienced a strain of 10 (except for the case of De_I = 0.1, a strain of 5 was used because 10 units of strain cannot be attained under this very small applied strain rate due to the limited observation time). Ensemble averages and standard deviations were calculated with the samples collected from all traces.

3. Dumbbell Model

3.1. Model Description. In addition to experiments, we construct a Brownian dumbbell model to obtain a qualitative description of DNA stretching in slitlike confinement. We model T4 DNA as two charged beads connected by an elastic spring. The dumbbell is placed in a homogeneous planar extensional electric field with its center of mass fixed at the stagnation point (see Figure 2C). According to the theorem of electrohydrodynamic equivalence proposed by Long et al.,[35] the electrophoretic stretching force $\mathbf{F}_E$ on each bead equals to the drag force exerted on the bead by a hydrodynamic flow in which the flow velocity is the same with the bead electrophoretic velocity in the electric field: $\mathbf{F}_E = \zeta(\mu\mathbf{E} - \mathbf{v}_{bead})$, where ζ, μ, and $\mathbf{v}_{bead}$ are the bead drag coefficient, bead electrophoretic mobility, and instantaneous velocity of the bead, respectively. The probability density function of the dumbbell end-to-end vector, $\psi(\mathbf{R},t)$, satisfies the diffusion equation[36]

$$\frac{\partial \psi}{\partial t} = -\frac{\partial}{\partial \mathbf{R}}\cdot\psi\left(\nabla\mu\mathbf{E}\cdot\mathbf{R} - \frac{2k_BT}{\zeta}\frac{\partial}{\partial \mathbf{R}}\ln\psi + \frac{2}{\zeta}\mathbf{F}_S\right) \quad (3)$$

where $\mathbf{R}$ is the dumbbell end-to-end vector and $\mathbf{F}_S$ is the elastic spring force (see Figure 2C). We seek steady-state solutions for ψ which allow us to predict the steady-state properties of the dumbbell such as the average end-to-end distance and the degree of extension fluctuations, as will be described later. Previous works[15,20,21,27] have employed similar models to study the coil−stretch transition of polymers in bulk in which case the drag coefficient varies with extension due to HI. Here the dumbbell model represents DNA molecule in thin channels where long-range HI is screened, and we assume the drag coefficient of the dumbbell to be constant. In addition, we neglect the dumbbell extension in the channel height dimension so that the dumbbell end-to-end distance ($R = |\mathbf{R}|$) satisfies $R^2 \approx {R_x}^2 + {R_y}^2$, where R_x and R_y are the dumbbell end-to-end distances in the x and y directions, respectively. For a planar homogeneous extensional electric field, the first term in parentheses on the right-hand side of eq 3 can be expressed as $\nabla\mu\mathbf{E}\cdot\mathbf{R} = (\partial/\partial\mathbf{R})[^1/_2\dot{\varepsilon}R^2\cos(2\theta)]$, where θ is the angle of the dumbbell principal axis with respect to the axis of elongation (see Figure 2C, $-\pi/2 < \theta < \pi/2$). The analytical solution to eq 3, for dumbbells at steady state such that $\partial\psi/\partial t = 0$, can now be found:[36]

$$\psi(\mathbf{R}) = K\exp\left\{\frac{1}{k_BT}\left[\frac{1}{4}\zeta\dot{\varepsilon}R^2\cos(2\theta) + \int_{\mathbf{R}}\mathbf{F}_S(\mathbf{R})\cdot d\mathbf{R}\right]\right\} \quad (4)$$

where K is the normalization constant which satisfies the condition $\int_{\mathbf{R}}\psi\, d\mathbf{R} = 1$.

3.2. Spring Force Law in Confinement. Information regarding the spring force law is required in order to compute the probability distribution function ψ using eq 4. Since confinement can either significantly reduce the spring force or have no impact on the spring force depending on the extension of the molecule, it is important that the spring force used in the dumbbell model accounts for these extension-dependent confining effects. The wormlike chain force law derived by Marko and Siggia[37] has usually been used to represent the spring force of DNA in bulk. The wormlike chain spring force is given by $\mathbf{F}_{S,bulk} = -H_{bulk}\mathbf{R}f(R/L_c)$, where L_c is the contour length of the spring and H_{bulk} is the unconfined Hookean spring constant which can be expressed in terms of L_c and the Kuhn step size b as $H_{bulk} = 3k_BT/L_cb$. The dimensionless function $f(R/L_c)$ in the force law describes the nonlinear response of the spring

$$f\left(\frac{R}{L_c}\right) = \frac{L_c}{6R}\left[\left(1 - \frac{R}{L_c}\right)^{-2} + \frac{4R}{L_c} - 1\right] \quad (5)$$

At low extensions ($R/L_c \ll 1$), f is approximately unity and the spring force becomes linear with extension: $\mathbf{F}_{S,bulk} \approx -H_{bulk}\mathbf{R}$. Considering that the DNA spring force is affected by the steric confinement only at these small extensions where the nonlinearity represented by f is not important, we assume that confinement primarily contributes to modifying the spring constant. Hence, we adapt the bulk wormlike chain spring force law to the confined case and use an extension-dependent spring constant H to represent the confinement-induced effects: $\mathbf{F}_S = -H(R)\mathbf{R}f(R/L_c)$. At large extensions where DNA is not stertically confined, the spring force remains identical to the bulk force law and $H = H_{bulk}$. At extensions very close to equilibrium, confined DNA exhibits linear spring force law with a reduced spring constant which we denote as the low-extension spring constant H_{low} ($H_{low} < H_{bulk}$). A transition region exists where the spring constant H gradually changes from H_{low} to H_{bulk} with increasing extension.

We seek the value of the spring constant H as a function of the dumbbell extension for all three channels used in this study. The 2 μm tall channel does not significantly confine T4 DNA[14] so that $H = H_{bulk}$ at all extensions. In the 300 and 150 nm tall channels, DNA is confined near equilibrium and H is extension-dependent. In order to obtain the functional form of H with respect to the dumbbell extension, we consider the fact that any modifications of the spring constant directly manifest themselves in the DNA relaxation dynamics, which can be measured experimentally by stretching T4 DNA molecules to nearly full extension using a high electric field gradient, turning off the field, and monitoring the evolution of the mean-square extension of these molecules.[14] Consequently, we can use the experimental relaxation data to infer the spring constant in confinement. We first examine the effects of an extension-dependent spring constant on the relaxation of an initially stretched dumbbell. The equation of change for the mean-square dumbbell end-to-end distance $\langle R^2\rangle$ can be derived from the diffusion equation (eq 3) by setting no electric field, multiplying the equation by R^2, and integrating over all the configuration space:[36]

$$\frac{d}{dt}\langle R^2\rangle = \frac{8k_BT}{\zeta} + \frac{4}{\zeta}\langle \mathbf{F}_S \cdot \mathbf{R}\rangle \tag{6}$$

We examine the relaxation behavior at extensions where H is affected by confinement. In both the 300 and 150 nm tall channels, the deviation of H from H_{bulk} occurs within the bulk linear force regime[14] so we employ the simplified spring force law $\mathbf{F}_S = -H\mathbf{R}$ to eq 6. We further assume fluctuation of the dumbbell end-to-end distance is small during the relaxation process such that $\langle HR^2\rangle \approx H\langle R^2\rangle$, giving

$$\frac{d}{dt}\langle R^2\rangle = \frac{8k_BT}{\zeta} - \frac{4H}{\zeta}\langle R^2\rangle \tag{7}$$

When the dumbbell has reached equilibrium such that $H = H_{low}$ and $d\langle R^2\rangle_{eq}/dt = 0$, the mean-square equilibrium end-to-end distance of the dumbbell can be solved from eq 7: $\langle R^2\rangle_{eq} = 2k_BT/H_{low}$. Substituting this result into eq 7 and defining a dimensionless dumbbell end-to-end distance $X = R/L_c$ and a scaled relaxation function $G = \langle X^2\rangle - \langle {X_{eq}}^2\rangle$, we arrive at

$$\frac{dG}{dt} = -\frac{4H}{\zeta}G - \frac{4(H - H_{low})}{\zeta}\langle {X_{eq}}^2\rangle \tag{8}$$

At high extensions where $X \gg X_{eq}$ and $H = H_{bulk}$, the second term on the right-hand side of eq 8 can be neglected, and the relaxation of G follows a single-exponential decay $dG/dt = -G/\tau_I$, where τ_I is the higher-extension relaxation time given by $\tau_I = \zeta/4H_{bulk}$. Similarly, for molecules close to equilibrium, $H = H_{low}$, the second term on the right-hand side of eq 8 vanishes, and the decay of G is also exponential with a single time constant $\tau_{II} = \zeta/4H_{low}$ which we term as the low-extension relaxation time. The prediction of two distinct relaxation time constants by eq 8 is in accord with recent experimental results of DNA relaxation times in confinement.[14,17]

Equation 8 can be rearranged to give

$$\frac{4H}{\zeta} = -\frac{1}{\langle X^2\rangle}\frac{dG}{dt} + \frac{1}{\tau_{II}}\frac{\langle {X_{eq}}^2\rangle}{\langle X^2\rangle} \tag{9}$$

Multiplying eq 9 by τ_I and considering the bead drag coefficient ζ is assumed to be a constant for a given channel height, we obtain

$$\frac{H}{H_{bulk}} = -\frac{\tau_I}{\langle X^2\rangle}\frac{dG}{dt} + \frac{\tau_I}{\tau_{II}}\frac{\langle {X_{eq}}^2\rangle}{\langle X^2\rangle} \tag{10}$$

Equation 10 allows us to calculate the spring constant from the relaxation data measured in experiments. We first located on experimental data (see Figure 3A,B) the two regions where G decays as a single-exponential function and extracted the corresponding time constants τ_I and τ_{II}, following procedures described previously.[17] Results of the relaxation times for all three channels are summarized in Table 1 (see Supporting Information for a comparison between the relaxation times of T4 DNA measured here and these reported in ref 14 for the same channel heights). The low-extension spring constant H_{low} is given by $H_{low}/H_{bulk} = \tau_I/\tau_{II}$. We next evaluated the first-order time derivative of the relaxation function and finally used eq 10 to calculate the spring constant in the transition region where H varies with extension. As a result, the above approach of relating the dumbbell model relaxation to experimental relaxation data directly gives the value of H_{low} and, more importantly, the quantitative extension dependence of the spring constant in terms of a smooth transition region.

Figure 3C and 3D show the extracted spring constant (normalized by H_{bulk}) as a function of the dumbbell end-to-end extension X for all three channels and the resulting spring force laws, respectively. It is clearly seen that the nanochannels change both the magnitude and the functional form of the spring force within the bulk linear force regime ($0 \le X < 0.3$). At small extensions, we observe a second linear force regime corresponding to sterically confined DNA with a reduced spring constant H_{low}. This confined linear regime is connected to a truncated bulk linear force regime present at larger extensions through a rather wide transition region where the spring force increases nonlinearly with X toward the bulk force law. The nonlinearity of the spring in the transition region primarily results from the gradual increase of the spring constant from H_{low} to H_{bulk}. A decrease in channel height not only lowers the value of H_{low} but also broadens both the confined linear force regime and the transition region. Consequently, the steric confining effects hold for a larger range of extensions (i.e., H restores to H_{bulk} at a larger extension) in the more confined channel, in agreement with previous scaling analysis.[17] In the 150 nm tall channel, the extension at which transition region terminates has been pushed up very close to $X = 0.3$. We expect that with further decrease in channel height the transition region will eventually extend into the nonlinear regime, and

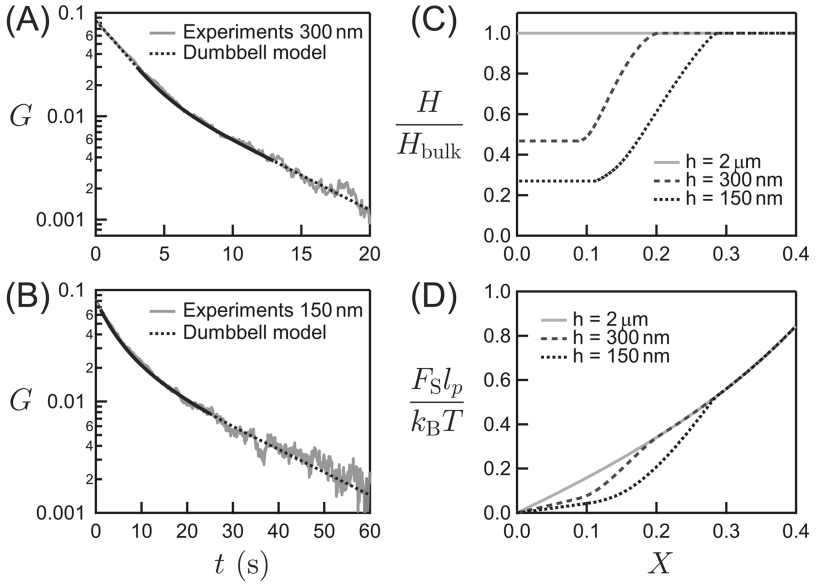

Figure 3. (A, B) Experimental relaxation data and relaxation of the dumbbell model calculated using eq 8 with the extracted spring constant for the 300 nm tall channel (A) and the 150 nm tall channel (B). The two regions where H is a constant are indicated with dotted lines and the transition region where H varies with extension is indicated with the black solid line in the dumbbell relaxation curve. (C) The ratio H/H_{bulk} as a function of the dimension less dumbbell end-to-end distance X extracted from experimental relaxation data for the 2 μm, 300 nm, and 150 nm tall channels. (D) The corresponding dimensionless dumbbell spring force $F_S l_p/k_B T$ as a function of X for the three channels; l_p is the persistence length of the DNA.

Table 1. Channel Dimensions and T4 DNA Relaxation Times

h	l (μm)	w (μm)	τ_I (s)	τ_{II} (s)
2.0 μm	100	40	1.9	1.9
300 nm	50	40	3.0	6.4
150 nm	50	40	5.7	21.2

the confined linear force regime will become the only linear region in the spring force law. We note that the spring force used in the dumbbell model represents the global effective spring force of a real DNA chain, which is the compound effect of the polymer's intrinsic entropic elasticity and the repulsive interactions among monomers (i.e., intramolecular excluded volume forces). The intrinsic spring constant (i.e., neglecting excluded volume effect) of a completely 2D chain is two-thirds that of a 3D bulk chain.[38] However, we observe that the effective spring force law can decrease by more than 50% compared to the bulk value. The excluded volume effect, therefore, should be playing an important role.

Now we have all the information needed to compute the dumbbell configuration probability density function ψ. We rewrite eq 4 in terms of dimensionless parameters and finally arrive at the equation that is used to calculate ψ:

$$\psi(X,\theta) = K \exp\left\{ -3N\left(\int_0^X \frac{H}{H_{bulk}} x f(x)\, dx - De_I X^2 \cos(2\theta) \right) \right\} \quad (11)$$

where N is the number of Kuhn steps in the spring $N = L_c/b$, and the dimensionless group De_I is the Deborah number defined using the higher extension relaxation time $De_I = \dot{\varepsilon}\tau_I$.

3.3. Predicting Experimental Observables. The probability density function ψ can be used to predict the steady-state properties of the dumbbell for given values of Deborah number De_I. We focus on three important properties that characterize the coil−stretch transition: the average extension, the degree of extension fluctuations, and the molecular orientation in the extensional electric field. However, the dumbbell model is used to represent the end-to-end vector of a real DNA chain which is not experimentally observable. Instead, the maximum extension R_{max} of the DNA was measured in experiments. We use X_{max} to denote the fractional maximum extension of the DNA: $X_{max} = R_{max}/L_c$. At large De_I where DNA molecules are highly extended, the maximum extension and the end-to-end distance are almost identical and share similar distributions. At low De_I where DNA molecules do not significantly deviate from equilibrium, the distributions of X_{max} can be quite different from the distribution of X. Specifically, we expect the end-to-end distance X to hold a lower average value and exhibit more fluctuations. In order to predict the behavior of the maximum extension, we constructed a special probability distribution function, $P(X_{max}|X)$, defined as the probability distribution of the maximum extension when the end-to-end distance of the molecule is fixed at a certain value. $P(X_{max}|X)$ was determined using Brownian dynamics simulations of a multi bead−spring model (see Supporting Information for details). This function allows us to map the dumbbell model prediction for X to the distribution of the maximum extension, $P(X_{max})$:

$$P(X_{max}) = \int_0^1 P(X_{max}|X)\, dX \int_{-\pi/2}^{\pi/2} \psi(X,\theta) X\, d\theta \quad (12)$$

The average fractional maximum extension can now be computed using

$$\langle X_{max} \rangle = \int_0^1 X_{max} P(X_{max})\, dX_{max} \quad (13)$$

We calculated the standard deviation (σ) of X_{max} to indicate the magnitude of extension fluctuations.

$$\sigma = \sqrt{\int_0^1 (X_{max} - \langle X_{max} \rangle)^2 P(X_{max})\, dX_{max}} \quad (14)$$

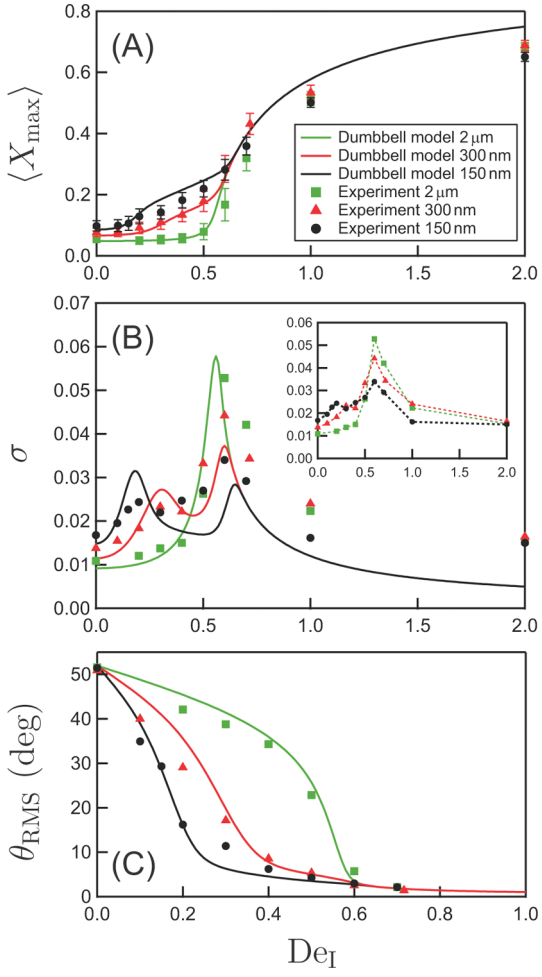

Figure 4. Experimental results and the dumbbell model predictions of the steady-state DNA behaviors. (A) The ensemble average steady-state maximum extension. (B) The standard deviation of the maximum extension which is a direct indication of the degree of extensional fluctuations; inset shows just the experimental standard deviation data for better clarity. (C) The root-mean-square angle of the principal axis of the molecule relative to the axis of elongation (θ_{RMS}, in degrees). All quantities are plotted against De_I.

The orientation of the DNA in the stretching electric field has been experimentally examined by measuring the root-mean-square angle (θ_{RMS}, see Figure 2B) of the principal axis of the DNA radius of gyration.[14] We thus calculated the same quantity for the dumbbell model:

$$\theta_{RMS} = \sqrt{\int_0^1 \int_{-\pi/2}^{\pi/2} \theta^2 \psi(X,\theta) X \, dX \, d\theta} \qquad (15)$$

In the T4 DNA relaxation experiments described earlier, we also only measured the maximum extension of DNA. We transformed the measured mean-square maximum extension $\langle X_{max}^2 \rangle$ into the square end-to-end distance X^2 so that eq 10 can be applied to calculate H. With the function $P(X_{max}|X)$, the mean-square maximum extension corresponding to a certain end-to-end distance X can be determined: $\langle X_{max}^2 \rangle = \int_0^1 X_{max}^2 P(X_{max}|X) \, dX_{max}$. The transformation was performed by simply seeking backward for the square end-to-end distance X^2 at a given $\langle X_{max}^2 \rangle$.

4. Results and Discussion

4.1. Steady-State Extension. Figure 4 shows both the experimental results and dumbbell model predictions for the steady-state properties of T4 DNA molecules (contour length $L_c \approx 75$ μm). All quantities are plotted against De_I, the Deborah number using the higher-extension relaxation time (τ_I) to normalize the strain rate. Figure 3A presents the average maximum fractional extensions of T4 DNA for the three channels with different heights. The experimental data collapse at large De_I, confirming that τ_I is the correct time scale that governs DNA stretching in confinement at large extensions.[14] At small values of De_I, DNA molecules in the nanochannels clearly exhibit a distinct deformation process comparing with molecules in the 2 μm tall channel which does not significantly confine T4 DNA. While a rather abrupt increase in extension is observed near $De_I = 0.5$ in the 2 μm tall channel, the coil−stretch transition becomes more gradual in confinement: the onset of DNA stretching occurs much earlier, and the sharpness of the transition reduces with decreasing channel height. The dumbbell model qualitatively predicts the stretching of DNA in confinement. Specifically, the predicted coil−stretch transitions agree almost quantitatively with experimental data at low De_I, and the extension curves corresponding to different channel heights collapse at high De_I. The model overpredicts DNA extension at large stretch, possibly due to the fact that the dumbbell model overestimates the stretching force by representing a continuous polymer with two beads positioned at the polymer's termini, which are subject to stronger field strengths than a majority of the polymer in between.

4.2. Extension Fluctuations. A unique feature accompanying the coil−stretch transition is the greatly enhanced conformation fluctuations near the critical strain rate.[22] We probe the steady-state extension fluctuations of T4 DNA by measuring the standard deviation (σ) of the fractional maximum extension. Results of σ as a function of De_I are displayed in Figure 4B. A single peak is clearly observed in the experimental standard deviation plot for DNA in the 2 μm tall channel (see inset of Figure 4B). The peak occurs at $De_I \approx 0.6$, in good agreement with that reported in a similar study for T4 DNA in bulk hydrodynamic elongational flow performed by Gerashchenko and Steinberg.[22] The magnitude of the peak measured in their study, however, is about 1.7-fold larger than that observed here for the same DNA in the 2 μm tall channel. We believe that a probable reason for this disparity is the much stronger extension dependence of the drag coefficient of DNA in bulk due to dominant intramolecular HI (see Supporting Information for details). The location of the peak in σ for the 2 μm tall channel also corresponds well to where the drastic increase in extension is seen in Figure 4A. In fact, the maxima of the standard deviation provide a quantitative criterion for the determination of the critical strain rates in the coil−stretch transition,[22] which, for the confined case, can be difficult to identify from the more gradual increase in extension.

The standard deviation data for DNA in the nanochannels show dramatically different characteristics. The peak at $De_I \approx 0.6$ still exists but has a lower amplitude in the more confined channel. More importantly, we observe increased fluctuations at equilibrium (i.e., $De_I = 0$) and the emergence of a second small peak at lower values of De_I. As the channel height decreases, the value of this local maximum increases and its location moves toward smaller De_I (peak occurs at $De_I \approx 0.3$ in the 300 nm tall channel and $De_I \approx 0.2$ in the 150 nm tall channel). The existence of a second peak suggests that the coil−stretch transition in these nanochannels is characterized by two critical strain rates, a phenomenon unique to confinement in polymer rheology. The dumbbell model confirms the shift from a single critical strain rate in

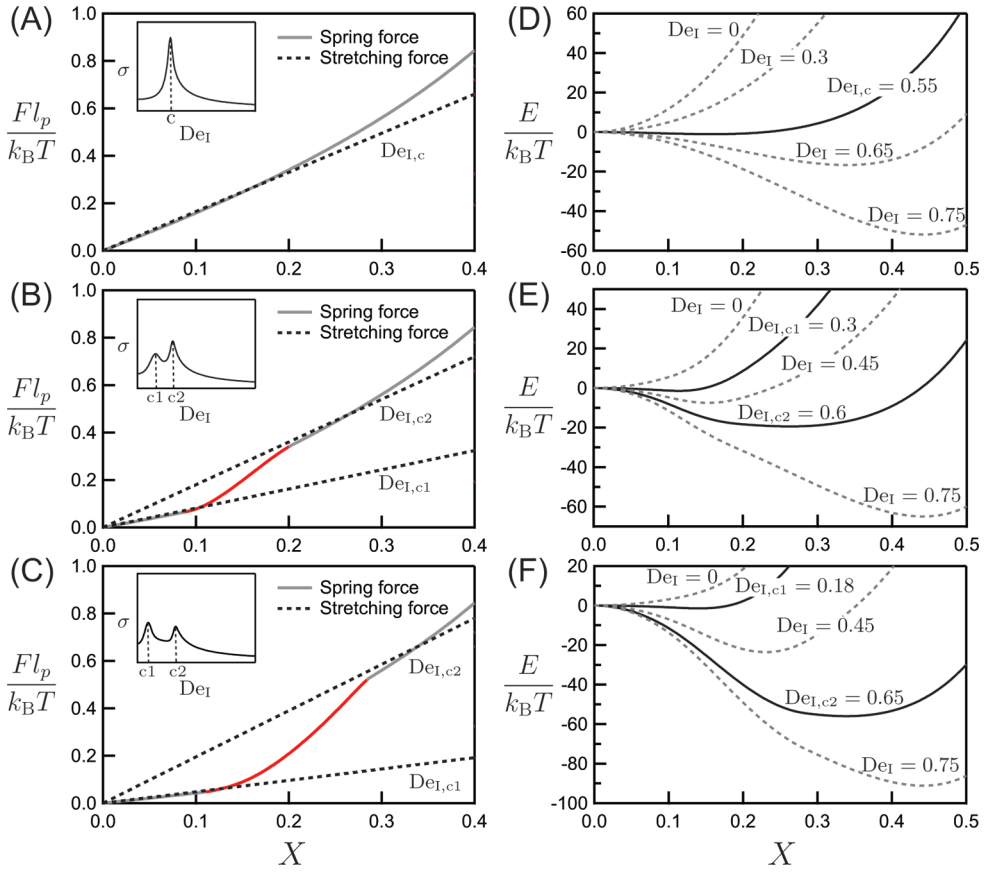

Figure 5. (A−C) Comparison between the stretching force exerted on a dumbbell with $\theta = 0$ at the critical De_I and the dumbbell spring force, for the 2 μm tall channel (A), the 300 nm tall channel (B), and the 150 nm tall channel (C). Both forces are nondimensionalized with k_BT/l_p. The red lines in (B) and (C) indicate the transition regions of the spring force where the spring constant increases with X. Insets show the dumbbell model prediction of the standard deviation σ versus De_I for corresponding channel heights. The critical Deborah number is determined by seeking local maxima of σ for each channel. A single critical Deborah number $De_{I,c}$ exists in the 2 μm tall channel while there are two critical Deborah numbers for the nanochannels, $De_{I,c1}$ and $De_{I,c2}$. (D−F) The effective conformational energy (E/k_BT) of the dumbbell as a function of X at different values of De_I for the 2 μm tall channel (D), the 300 nm tall channel (E), and the 150 nm tall channel (F). The energy landscapes at the critical Deborah numbers in each channel are highlighted with the black solid lines.

the microchannel to two critical strain rates in confinement. The predicted values of the critical De_I corresponding to the local maxima in σ match experiments well. Effects of the channel heights on the magnitude of these peaks and the equilibrium fluctuations are also qualitatively captured in the model. However, the dumbbell model overpredicts the magnitude of the peak near equilibrium and underpredicts that at the larger De_I. Considering that the dumbbell model is a very simplistic description of a real DNA molecule, we would expect some moderate quantitative differences.

4.3. Molecular Orientation in the Extensional Electric Field. Figure 4C shows the root-mean-square angle (θ_{RMS}) of the principal axis of the in-plane DNA radius of gyration versus De_I. θ_{RMS} indicates the degree of alignment toward the axis of elongation (x-axis) from the equilibrium average of $\theta_{RMS,eq} = 52°$. Highly extended molecules align completely with the stretching electric field and give $\theta_{RMS,eq} = 0°$ (see Figure 2B). It is clearly seen that DNA molecules start to orient toward the x-axis at very low values of De_I and yield strong measurable response of θ_{RMS}. Both the experimental data and the dumbbell model predictions show dramatically faster alignment of DNA molecules with the stretching electric field in the nanochannels. In all three channels, the molecules have already become fairly aligned with the stretching field at the Deborah number where significant stretching occurs or the first peak in the standard deviation emerges, indicating that this orientational response characterizes the behaviors departing from equilibrium dynamics prior to coil−stretch transition.[14] The molecule must first align with the field in order to be deformed, and the faster molecular orientation in the nanochannels is thus in accord with the earlier onset of stretching observed in Figure 4A.

4.4. Force Balance and Effective Conformational Energy. Both the experiments and theory show that the coil−stretch process is qualitatively different in confinement and the existence of two critical Deborah numbers. Further insight can be gained by revisiting the dumbbell model and considering both a force balance and effective conformational energy landscape. The conformation of a polymer in an elongational field is a competition between the spring force and the stretching force (electric field). The counterbalance between these two forces can be further related to an effective conformational energy landscape, which is very useful for the interpretation of the coil−stretch transition.[15,20,21,39,40] From eq 11, we can define an effective dumbbell conformational free energy E that satisfies $\psi \sim \exp(E/k_BT)$:

$$\frac{E(X,\theta)}{k_BT} = 3N\left[\int_0^X \frac{H}{H_{bulk}} xf(x)\,dx - De_I X^2 \cos(2\theta)\right] \quad (16)$$

We consider a dumbbell at steady-state and assume it is completely aligned with the axis of elongation ($\theta = 0$). The electrophoretic stretching force exerted on each bead now

varies linearly with the dumbbell extension: $F_E = {}^1/_2\zeta\dot{\varepsilon}R$. We nondimensionalize the force with k_BT/l_p, giving $\hat{F}_E = F_E l_p/k_BT = 3\mathrm{De}_I X$. The dimensionless spring force is given by $\hat{F}_S = F_S l_p/k_BT = (3/2)(H/H_{bulk})Xf(X)$ and reduces to $\hat{F}_S = (3/2)(H/H_{bulk})X$ at small values of X. The effective conformation energy of the dumbbell as a function of X is calculated with eq 16 by setting $\theta = 0$. Figure 5 shows the comparison between $\hat{F}_E$ at the critical Deborah numbers and the dumbbell spring force $\hat{F}_S$ for each channel as well as the corresponding effective conformational energy landscapes at several different values of De_I. The critical Deborah numbers are determined by seeking local maxima of the predicted standard deviations (see insets of Figure 5A−C): $\mathrm{De}_{I,c} = 0.55$ for the 2 μm tall channel, $\mathrm{De}_{I,c1} = 0.3$ and $\mathrm{De}_{I,c2} = 0.6$ for the 300 nm tall channel, and $\mathrm{De}_{I,c1} = 0.18$ and $\mathrm{De}_{I,c2} = 0.65$ for the 150 nm tall channel.

Figure 5A shows the force comparison for the 2 μm tall channel in which the bulk spring force law applies. It is clearly seen that the linear region of the spring force is balanced by the stretching force at the critical Deborah number. This force balance creates a flat effective energy profile within the entire bulk linear force regime (see Figure 5D), indicating that the dumbbell has equal probability to sample at any of these end-to-end extensions ($0 \leq X < 0.3$) and thus exhibits large extension fluctuations. At $\mathrm{De}_I < \mathrm{De}_{I,c}$, the stretching force is lower than the spring force at all extensions (except for $X = 0$) so the dumbbell remains collapsed. This collapsed state is also implied by the effective energy landscape which shows a single minimum at $X = 0$ at these small values of De_I. Once De_I is increased above $\mathrm{De}_{I,c}$, the stretching force becomes larger than the spring force within the linear force regime, and we observe the formation of a deep energy well with the minimum point now located at a much higher extension (beyond the linear force regime). As a result, the linear nature of the bulk spring force at small extensions induces this sudden shift in the location of the energy minimum and eventually leads to the sharp coil−stretch transition.

In the nanochannels, the presence of two linear regimes with different spring constants in the DNA spring law is responsible for the two critical strain rates in the coil−stretch transition. As shown in Figure 5B and 5C, the confined linear force regime at small extensions and the truncated bulk linear force regime at larger extensions are balanced by the stretching force at two different critical Deborah numbers, $\mathrm{De}_{I,c1}$ and $\mathrm{De}_{I,c2}$, respectively. The force balance is clearly seen at $\mathrm{De}_{I,c1}$ but less evident at $\mathrm{De}_{I,c2}$, especially for the 150 nm tall channel. Alternatively, the effective energy landscape can provide a much clearer demonstration of this force balance because the exact superposition of the stretching force and the spring force is not required for a relatively flat energy profile: we observe in Figure 5E and 5F that the energy landscape becomes flat within the range of extensions where the magnitudes of $\hat{F}_E$ and $\hat{F}_S$ are close to each other at both critical Deborah numbers. Early stretching occurs once the Deborah number exceeds $\mathrm{De}_{I,c1}$ as the effective energy starts to show a clear minimum at $X > 0$. The stretching process, however, is limited by the nonlinear transition region of the spring force (indicated as the red lines in Figure 5B,C). For Deborah numbers between $\mathrm{De}_{I,c1}$ and $\mathrm{De}_{I,c2}$, the nonlinear spring force restricts the locations of the energy minimum to extensions within the transition region and thus results in a more gradual increase in extension with De_I.

Using the simple scaling of $\hat{F}_E \sim \hat{F}_S$, we can estimate the values of the critical Deborah numbers for all three channel heights. For the 2 μm tall channel $H = H_{bulk}$, and thus $\hat{F}_S = {}^3/_2X$ in the linear force regime, giving $\mathrm{De}_{I,c} \sim 0.5$. For the nanochannels, the spring force is given by $\hat{F}_S = (3/2)(H_{low}/H_{bulk})X$ and $\hat{F}_S = {}^3/_2X$ in the two linear regimes, respectively. The resulting two critical Deborah numbers are $\mathrm{De}_{I,c1} \sim H_{low}/2H_{bulk}$ (this yields $\mathrm{De}_{I,c1} \sim 0.24$ for the 300 nm tall channel and $\mathrm{De}_{I,c1} \sim 0.13$ for the 150 nm tall channel) and $\mathrm{De}_{I,c2} \sim 0.5$. The estimations of the critical Deborah numbers from the scaling analysis are similar to these determined from the standard deviation data.

The magnitude of the steady-state extension fluctuation is directly linked to the flatness of the effective conformational energy landscape. From Figure 5D−F we see that as the channel height decreases, the effective energy for a molecule at equilibrium (i.e., $\mathrm{De}_I = 0$) shows a more gradual increase from $X = 0$ due to the reduced spring constant at these small extensions. As a result, a thermal disturbance ($\Delta E \sim k_BT$) produces a larger change in extension in the more confined channel, consistent with the enhanced equilibrium fluctuations observed in experiments. At the critical strain rates in each channel, the magnitude of the standard deviation σ is proportional to the span of extension over which the effective energy has a flat profile. Since the flat energy landscape results from the balance of the stretching force with the linear region of the spring force, the width of the corresponding linear spring force regime essentially determines the value of σ at these critical strain rates. A decrease in channel height broadens the confined linear force regime and narrows the truncated bulk linear force regime (see Figure 3D), leading to an increased peak in the standard deviation at $\mathrm{De}_{I,c1}$ and a suppressed peak at $\mathrm{De}_{I,c2}$, as observed in Figure 4B. Finally, we point out that the existence of two critical strain rates in the coil−stretch transition requires two distinct ranges of extensions where the spring force keeps strong linearity. As discussed in section 3.2, further decrease in the channel height from 150 nm may push the transition region into the nonlinear regime of the spring force (i.e., $X > 0.3$), and the resulting spring force law returns to possessing a single linear force regime. Under this condition, we postulate that a single peak in the standard deviation exists at $\mathrm{De}_{I,c} \sim H_{low}/2H_{bulk}$, and the coil−stretch transition is again characterized by a single critical strain rate. These effects of further confinement are yet to be examined.

5. Conclusions

We have used a nanofluidic cross-slot device to investigate the influence of slitlike confinement on the coil−stretch transition of single DNA molecules in a 2D homogeneous extensional electric field. We examine the evolution of three steady-state properties with applied strain rate that characterize the coil−stretch transition: the average extension, the magnitude of extension fluctuations, and the molecular orientations in the extensional electric field. Comparing with the sharp transition occurred near a single critical strain rate in the unconfined case, DNA molecules in the nanochannels exhibit highly modified coil−stretch processes. Specifically, the onset of DNA stretching starts earlier, the transition progresses more gradually, and most importantly, we identify two distinct critical strain rates in the transition. Prior to the conformation transition, DNA shows much faster alignment with the stretching electric field in the nanochannels. We have constructed a Brownian dumbbell model in which the confinement effects are represented with a constant drag coefficient and an extension-dependent spring constant extracted from experimental relaxation data. The dumbbell model is able to provide qualitative predictions of the coil−stretch transition of DNA in confinement. By exploring the interplay between the stretching force and the spring force as well as the effective energy landscape of the dumbbell model, we conclude that the essential physical

reason for the different coil−stretch transition is the altered DNA spring force law which for the channel heights studied here contains two linear force regimes with distinct spring constants. Further experiments should be performed to explore the effects of even stronger confinement. Our results are not only of fundamental importance to the understanding of the interactions between confinement and a deforming polymer but also useful in the design of devices aiming to exploit confinement to manipulate DNA molecules.

Acknowledgment. The authors thank the Singapore-MIT Alliance for Research and Technology (SMART) for funding, the National Science Foundation Grant CBET-0852235, and Award No. T32EB006348 from the National Institute of Biomedical Imaging and Bioengineering. The content is solely the responsibility of the authors and does not necessarily represent the official views of the National Institute of Biomedical Imaging and Bioengineering or the National Institutes of Health.

Supporting Information Available: Description of the electric field characterization experiments; comparison between the T4 DNA relaxation times measured here and these reported previously in ref 14; description of the Brownian dynamics simulation method used to compute $P(X_{max}|X)$; demonstration of a dumbbell model with extension-dependent drag coefficient. This material is available free of charge via the Internet at http://pubs.acs.org.

References and Notes

(1) Han, J.; Craighead, H. G. *Science* **2000**, *288*, 1026.
(2) Doyle, P. S.; Bibette, J.; Bancaud, A.; Viovy, J.-L. *Science* **2002**, *295*, 2237.
(3) Chan, E. Y.; Goncalves, N. M.; Haeusler, R. A.; Hatch, A. J.; Larson, J. W.; Maletta, A. M.; Yantz, G. R.; Carstea, E. D.; Fuchs, M.; Wong, G. G.; Gullans, S. R.; Gilmanshin, R. *Genome Res.* **2004**, *14*, 1137.
(4) Jo, K.; Dhingra, D. M.; Odijk, T.; de Pablo, J. J.; Graham, M. D.; Runnheim, R.; Forrest, D.; Schwartz, D. C. *Proc. Natl. Acad. Sci. U.S.A.* **2007**, *104*, 2673.
(5) Brochard, F.; de Gennes, P. G. *J. Chem. Phys.* **1977**, *67*, 52.
(6) Daoud, M.; de Gennes, P. G. *J. Phys.* (*Paris*) **1977**, *38*, 85.
(7) Brochard, F. *J. Phys.* (*Paris*) **1977**, *38*, 1285.
(8) Odijk, T. *Macromolecules* **1983**, *16*, 1340.
(9) Guo, L. J.; Cheng, X.; Chou, C. F. *Nano Lett.* **2004**, *4*, 69.
(10) Reisner, W.; Morton, K. J.; Riehn, R.; Wang, Y. M.; Yu, Z. N.; Rosen, M.; Sturm, J. C.; Chou, S. Y.; Frey, E.; Austin, R. H. *Phys. Rev. Lett.* **2005**, *94*, 196101.
(11) Mannion, J. T.; Reccius, C. H.; Cross, J. D.; Craighead, H. G. *Biophys. J.* **2006**, *90*, 4538.
(12) Douville, N.; Huh, D.; Takayama, S. *Anal. Bioanal. Chem.* **2008**, *391*, 2395.
(13) Zhang, C.; Zhang, F.; van Kan, J. A.; van der Maarel, J. R. C. *J. Chem. Phys.* **2008**, *128*, 225109.
(14) Balducci, A. G.; Tang, J.; Doyle, P. S. *Macromolecules* **2008**, *41*, 9914.
(15) de Gennes, P. G. *J. Chem. Phys.* **1974**, *60*, 5030.
(16) Hsieh, C.-C.; Doyle, P. S. *Korea-Aust. Rheol. J.* **2008**, *20*, 127.
(17) Balducci, A.; Hsieh, C. C.; Doyle, P. S. *Phys. Rev. Lett.* **2007**, *99*, 238102.
(18) Perkins, T. T.; Smith, D. E.; Chu, S. *Science* **1997**, *276*, 2016.
(19) Smith, D. E.; Chu, S. *Science* **1998**, *281*, 1335.
(20) Schroeder, C. M.; Babcock, H. P.; Shaqfeh, E. S. G.; Chu, S. *Science* **2003**, *301*, 1515.
(21) Schroeder, C. M.; Shaqfeh, E. S. G.; Chu, S. *Macromolecules* **2004**, *37*, 9242.
(22) Gerashchenko, S.; Steinberg, V. *Phys. Rev. E* **2008**, *78*, 040801(R).
(23) Juang, Y. J.; Wang, S.; Hu, X.; Lee, L. J. *Phys. Rev. Lett.* **2004**, *93*, 268105.
(24) Tang, J.; Doyle, P. S. *Appl. Phys. Lett.* **2007**, *90*, 224103.
(25) Larson, R. G.; Magda, J. J. *Macromolecules* **1989**, *22*, 3004.
(26) Vincenzi, D.; Bodenschatz, E. *J. Phys. A* **2006**, *39*, 10691.
(27) Celani, A.; Puliafito, A.; Vincenzi, D. *Phys. Rev. Lett.* **2006**, *97*, 118301.
(28) Bakajin, O. B.; Duke, T. A. J.; Chou, C. F.; Chan, S. S.; Austin, R. H.; Cox, E. C. *Phys. Rev. Lett.* **1998**, *80*, 2737.
(29) Balducci, A.; Mao, P.; Han, J. Y.; Doyle, P. S. *Macromolecules* **2006**, *39*, 6273.
(30) Hsieh, C.-C.; Balducci, A.; Doyle, P. S. *Macromolecules* **2007**, *40*, 5196.
(31) Deen, W. M. *Analysis of Transport Phenomena*; Oxford University Press: New York, 1998.
(32) Randall, G. C.; Doyle, P. S. *Proc. Natl. Acad. Sci. U.S.A.* **2005**, *102*, 10813.
(33) Mao, P.; Han, J. Y. *Lab Chip* **2005**, *5*, 837.
(34) Hsieh, C.-C.; Balducci, A.; Doyle, P. S. *Nano Lett.* **2008**, *8*, 1683.
(35) Long, D.; Dobrynin, A. V.; Rubinstein, M.; Ajdari, A. *J. Chem. Phys.* **1998**, *108*, 1234.
(36) Bird, R. B.; Curtiss, C. F.; Armstrong, R. C.; Hassager, O. *Dynamics of Polymeric Liquids*, 2nd ed.; Wiley-Interscience: New York, 1987; Vol. *2*.
(37) Marko, J. F.; Siggia, E. D. *Macromolecules* **1995**, *28*, 8759.
(38) Rubinstein, M.; Colby, R. H. *Polymer Physics*; Oxford University Press: New York, 2003.
(39) Beck, V. A.; Shaqfeh, E. S. G. *J. Chem. Phys.* **2006**, *124*, 094902.
(40) Beck, V. A.; Shaqfeh, E. S. G. *J. Rheol.* **2007**, *51*, 561.